Coherent and incoherent scattering by oceanic bubbles

K. Sarkar and A. Prosperetti

Department of Mechanical Engineering, The Johns Hopkins University, Baltimore, Maryland 21218

A substantial amount of research on acoustic scattering by underwater bubbles is based on the theory of incoherent scattering. More recent work, devoted to much denser bubble assemblies, has instead used effective-media formulations that presuppose coherent effects. Here the mutual relationship between the two approaches is elucidated. It is shown that, underlying the incoherent results, is a WKB approximate solution of the effective equations. As an application, the scattering by tenuous subsurface bubble layers and acoustical bubble counting techniques are examined. Significant differences with previous results are found.

INTRODUCTION

Bubble clouds have recently become of great interest to the underwater acoustics community due to their possible role in the production and scattering of low-frequency (from a fraction of a kHz to several kHz) noise (Carey and Bradley, 1985; Carey and Browning, 1988; Prosperetti *et al.*, 1993; Sarkar and Prosperetti, 1993). The mechanism by which these effects are produced involves the acoustic excitation of the cloud as a whole rather than of the individual constituent bubbles. Accordingly, the theoretical tools adapted for the analysis have been found in the theory of nonhomogeneous media in which the bubbly liquid is treated, in an average sense, as a continuum and the individuality of the bubbles lost.

While this theory has been very successfully compared with experiment (Commander and Prosperetti, 1989; Yoon *et al.*, 1991; Nicholas *et al.*, 1994), it represents a departure from the way in which oceanic bubble phenomena have usually been analyzed in the past, when the emphasis was on higher frequencies (tens of kHz and above) and sparser bubble assemblies. In that case the bubbles were treated as individual scatterers or emitters of sound and the relationship between the two points of view is not apparent. It is the purpose of the present paper to clarify this relationship. In so doing, the assumptions underlying the previous approaches will also be clarified and their limitations explored in the light of a more accurate theory.

In part, the differences between the two approaches must be attributed to the differences between coherent and incoherent scattering and emission. However, there are additional elements that make the comparison more interesting.

Although sound emission by individual bubbles is mentioned among the possible oceanic noise sources, little quantitative effort has been devoted to this aspect of bubble activity. Mostly, the previous studies have focused on the acoustic scattering properties of bubbles, and it is to these that the present analysis will be limited. The problems that we study are the high-frequency reverberation and back-scattering due to bubbles, and an acoustical technique of bubble counting.

I. COHERENT AND INCOHERENT SCATTERING

In this paper we shall only be concerned with random arrangements of scatterers. In this case, the basic physics underlying the coherent and incoherent interaction of waves with scatterers is well known (see e.g., Morse and Feshbach, 1953, p. 1494; Carey and Roy, 1993). Incoherent behavior dominates when the scatterers are separated by distances comparable with the wavelength or larger, and leads to a scattered intensity proportional to the number of scatterers N. When the scatterers are closely spaced, on the other hand, one observes coherent behavior with a much stronger scattering strength proportional to N^2. The transition between the two regimes is continuous: any random assembly of scatterers, however compact in its spatial extension, will give rise to an incoherent component which becomes (relatively) stronger and stronger as the typical acoustic wavelength decreases. Eventually, the incoherent component becomes dominant and the coherent field becomes small, although its vanishing is asymptotic rather than abrupt.

An alternative—but equivalent—description of the situation can be given in terms of ensemble averages. Imagine an ensemble of repeated scattering experiments in which the average conditions are nominally identical, and the only difference lies in the details of the spatial arrangement of the individual scatterers. Upon averaging the results (e.g., the spectra of the scattered signal) of all the experiments, one would obtain the coherent field, while the difference of the measured field in each experiment from the coherent average would correspond to the incoherent field for each particular experiment. The ensemble average of these incoherent fields vanishes by definition, but the ensemble average of the squares does not and this quantity is proportional to the incoherent scattering intensity.

The equivalence of the two descriptions stems essentially from the equivalence between volume and ensemble averaging for spatially homogeneous systems.

In the situations of concern in underwater acoustics the density of bubbles is generally small, with gas volume fractions ranging from perhaps 10^{-6} to a few percent. However, in view of the large compressibility and energy dissipation of bubbles, exceedingly strong effects on sound propagation take place near the upper end of this range.

II. FOLDY'S THEORY

In a pioneering paper published in 1945, Foldy developed a consistent theory of coherent and incoherent scatter-

ing. He showed that the coherent field $\langle p \rangle$—defined in terms of the average over an ensemble of realizations of the bubbles–water mixture—is the solution of a Helmholtz equation

$$(\nabla^2 + \kappa^2)\langle p \rangle = 0, \tag{1}$$

in which the position-dependent effective wave number κ is given by

$$\kappa^2 = k^2 + \int_{a_{\min}}^{a_{\max}} h(a,\omega;\mathbf{x})N(a,\mathbf{x})da. \tag{2}$$

Here the pressure perturbation has been assumed proportional to $\exp(i\omega t)$, $k = \omega/c$ is the wave number in the pure water (speed of sound c), a denotes the bubble radius, and $a_{\min}$ and $a_{\max}$ are the minimum and maximum values of this quantity. The position-dependent number density of bubbles per unit radius increment is denoted by N and h is the scattering form factor defined by

$$h(a,\omega;\mathbf{x}) = \frac{4\pi\omega^2 a}{\omega_0^2 - \omega^2 + 2ib\omega}. \tag{3}$$

Here ω_0 is the natural frequency of a bubble of radius a given by

$$\omega_0^2 = \frac{p_0}{\rho a^2}\left(\Re\Psi - \frac{2\sigma}{ap_0}\right), \tag{4}$$

and the effective damping parameter b is

$$b = \frac{2\mu}{\rho a^2} + \frac{p_0}{2\rho\omega a^2}\Im\Psi + \frac{\omega^2 a}{2c}. \tag{5}$$

In these expressions $\Re\Psi$ and $\Im\Psi$ denote the real and imaginary parts of the complex function $\Psi(\chi)$ defined by

$$\Psi = \frac{3\gamma}{1 - 3(\gamma-1)i\chi[(i/\chi)^{1/2}\coth(i/\chi)^{1/2}-1]}, \tag{6}$$

with γ the ratio of specific heats of the gas (air), $\chi = D/(\omega a^2)$, and D the gas thermal diffusivity. The equilibrium pressure in the bubble, p_0, is related to the undisturbed ambient pressure p_∞ by $p_0 = p_\infty + 2\sigma/a$ and μ denotes the liquid viscosity, ρ its density, and σ the interfacial tension. For a more detailed explanation and derivation of these formulae see Prosperetti et al. (1988), Commander and Prosperetti (1989), or Prosperetti (1991). Equation (3) may be recast in the more familiar-looking form

$$h = \frac{4\pi a}{(\omega_0/\omega)^2 - 1 + i\delta}, \tag{7}$$

where the logarithmic decrement is given by $\delta = 2b/\omega$. This form has however the disadvantage of hiding the strong frequency dependence of ω_0 and b. Graphs of δ as a function of the equilibrium radius have been given by Medwin (1977a; see also Clay and Medwin, 1991) and are also shown in Fig. 1 for different values of ω for a water–air system. These and all other numerical results in this paper are for air bubbles in water at standard temperature and pressure. Note that the position dependence of h arises from the fact that ω_0 and b depend on the local static pressure p_∞, which is a function of depth.
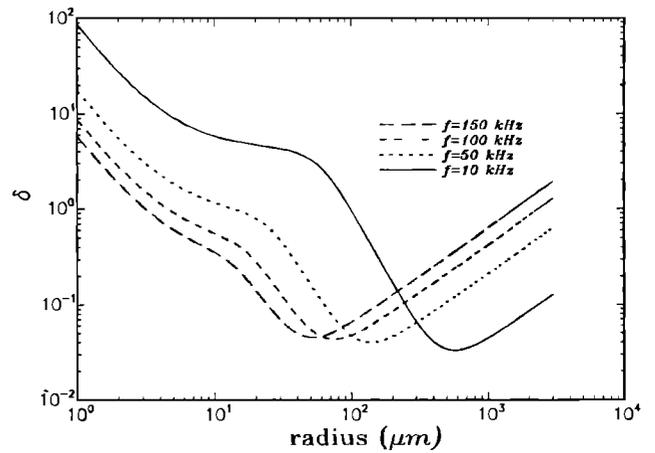
FIG. 1. The logarithmic decrement $\delta = 2b/\omega$ as a function of the bubble equilibrium radius a for several sound frequencies $f = \omega/2\pi$. For each frequency the resonant radius is near the minimum of the curve.

In the same 1945 paper Foldy obtained an integral equation for the incoherent field, the magnitude of which he defines as

$$|p_{\rm inc}|^2 = \langle |p|^2 \rangle - |\langle p \rangle|^2. \tag{8}$$

The equation is

$$\langle |p(\mathbf{x})|^2 \rangle = |\langle p(\mathbf{x}) \rangle|^2 + \frac{1}{4\pi}\int S_s(\mathbf{x}')$$
$$\times\langle |p(\mathbf{x}')|^2 \rangle|G(\mathbf{x},\mathbf{x}')|^2\, d^3x'. \tag{9}$$

Here

$$S_s(\omega,\mathbf{x}) = \int_{a_{\min}}^{a_{\max}} \sigma_s(a,\omega;\mathbf{x})N(a,\mathbf{x})da, \tag{10}$$

with σ_s the scattering cross section of a single bubble

$$\sigma_s = \frac{1}{4\pi}|h|^2 = \frac{4\pi a^2}{[(\omega_0/\omega)^2 - 1]^2 + \delta^2} \tag{11}$$

is the total scattering cross section per unit volume and G is the "dressed" Green's function of the Helmholtz equation, i.e., the Green's function corresponding to the mixture wave number κ rather than to the pure liquid wave number k,

$$[\nabla_x^2 + \kappa^2(\mathbf{x})]G = -4\pi\delta^{(3)}(\mathbf{x}-\mathbf{x}'). \tag{12}$$

This result of Foldy's, originally obtained on a somewhat heuristic basis, has been confirmed by the later work of Twersky (1964). In the presence of weak scattering effects, Eq. (9) can be approximately solved by using a Neumann series truncated at the first term (the Born approximation) to obtain

$$|p_{\rm inc}|^2 = \frac{1}{4\pi}\int S_s(\mathbf{x}')|\langle p(\mathbf{x}') \rangle|^2|G(\mathbf{x},\mathbf{x}')|^2\, d^3x'. \tag{13}$$

Equations (1), (12), and (13) constitute a closed mathematical model for the coherent and incoherent scattering from bubble distributions. We now show that the formulations used by earlier researchers (Clay and Medwin 1964; Crowther, 1980; McDaniel, 1987, and others) can be derived from this model with suitable approximations.

III. WKB APPROXIMATION

If we only consider tenuous bubble distributions with κ slowly varying over a wavelength, we can approximately solve Eqs. (1) and (12) by the WKB method. We must however prescribe a boundary condition at the ocean's surface. Previous investigators have completely neglected the presence of waves assuming the surface to be flat. We shall retain this model but, in order to account—however crudely—for waves, we shall assume that the reflected pressure wave has a phase ϕ with respect to the incident wave. In proposing this assumption we envisage a plane coinciding with the mean ocean surface position, with the actual surface position randomly above or below this mean level. The phase of the reflected "wavelet" from each surface element will therefore fluctuate about the value corresponding to the mean position, which we account for by ascribing a different value of ϕ to the wavelet. The amplitude of this fluctuation will be of the order of the product of the wave number and the significant wave height. If the latter is much greater than the acoustic wavelength (high frequencies), ϕ will have a range of variation of 2π or greater. In the opposite limit of low frequencies, on the other hand, the presence of surface waves is immaterial and $\phi \approx \pi$ to satisfy the condition $p=0$ at the free surface.

With this specification, with the assumption of rectilinear rays, a straightforward application of the lowest-order WKB approximation to the Helmholtz equation (1) for the coherent field $\langle p \rangle$ generated by a unit point source located at $\mathbf{R}$ gives

$$\langle p(\mathbf{x}) \rangle = \frac{1}{4\pi|\mathbf{x}-\mathbf{R}|} \exp\left(-i\int_\mathbf{R}^\mathbf{x} \kappa(\mathbf{y})dl_y\right)$$
$$+ \frac{\exp(i\phi)}{4\pi|\mathbf{x}-\mathbf{R}_r|} \exp\left(-i\int_{\mathbf{R}_r}^\mathbf{x} \kappa(\mathbf{y})dl_y\right), \quad (14)$$

where the subscript r indicates the point reflected in the surface. For the range of bubble concentrations of interest here, up to 0.1% by volume or so, the lowest-order WKB result embodied in this formula is sufficient. The rays are approximated by the straight line joining source and receiver and the integral in the first exponential is taken along this line, while that in the second exponential is taken along the line ABC of Fig. 2.

In a similar way we find the following approximate result for the Green's function G:

$$G(\mathbf{x},\mathbf{x}') = \frac{1}{|\mathbf{x}-\mathbf{x}'|} \exp\left(-i\int_{\mathbf{x}'}^\mathbf{x} \kappa(\mathbf{y})dl_y\right)$$
$$+ \frac{\exp(i\phi)}{|\mathbf{x}-\mathbf{x}'_r|} \exp\left(-i\int_{\mathbf{x}'_r}^\mathbf{x} \kappa(\mathbf{y})dl_y\right). \quad (15)$$

As before, the integral in the first exponential is along the straight line from $\mathbf{x}'$ to $\mathbf{x}$, while that in the second one is along a line similar to the line ABC of Fig. 2. The differential dl_y is the element of arc length along these paths, which ensures reciprocity of the Green's function.

In the application of the formula (13) to the case of backscattering, the argument $\mathbf{x}$ of the Green's function coincides with the source point $\mathbf{R}$ and, due to the symmetry of
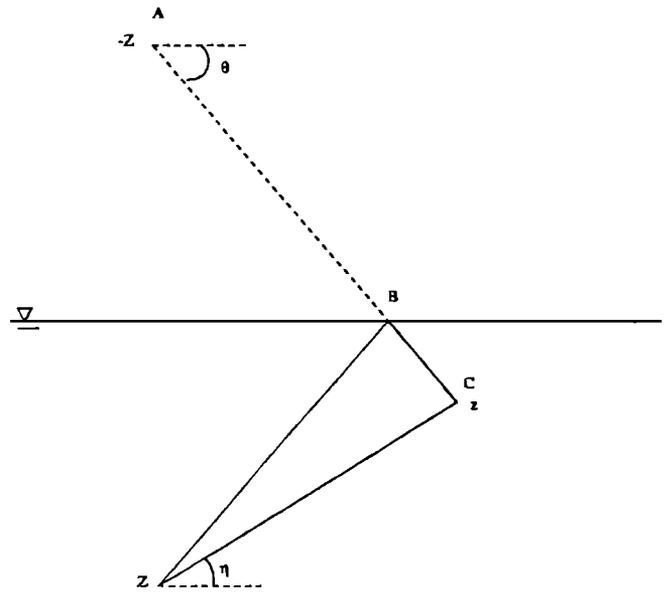
FIG. 2. Ray diagram for the derivation of the approximation (20).

the Green's function, also $G(\mathbf{R},\mathbf{x}')$ equals the field at $\mathbf{x}'$ produced by a unit source at $\mathbf{R}$, which is the same as $\langle p \rangle(\mathbf{x}')$. Hence we may write for the integrand in (13)

$$|\langle p \rangle(\mathbf{x}')|^2 |G(\mathbf{R},\mathbf{x}')|^2 = (4\pi)^2 |\langle p \rangle(\mathbf{x}')|^4. \quad (16)$$

In the applications that follow, as in McDaniel and Gorman (1982, 1983) and Vagle and Farmer (1992), we assume that the medium is stratified in the vertical direction so that, in the integrals appearing in (14) and (15), $dl_y = d\zeta/\sin \eta$, where $d\zeta$ is the differential in the vertical direction and η is the grazing angle, i.e., the angle that the ray connecting $\mathbf{R}$ with $\mathbf{x}'$ makes with the horizontal free surface. With this specification the first integral in (14) becomes

$$\int_\mathbf{R}^\mathbf{x} \kappa(\mathbf{y})dl_y = \frac{1}{\sin \eta} \int_Z^z \kappa(\zeta)d\zeta. \quad (17)$$

In order to have more compact expressions it is also useful to define

$$F(z) = \frac{2}{\sin \eta} \int_Z^z \kappa(\zeta)d\zeta. \quad (18)$$

As for the second integral in (14), with reference to Fig. 2, we have

$$\int_{\mathbf{R}_r}^\mathbf{x} \kappa(\mathbf{y})dl_y = \frac{1}{\sin \theta} \left(\int_Z^0 \kappa(\zeta)d\zeta - \int_0^z \kappa(\zeta)d\zeta\right), \quad (19)$$

where the angle θ is defined in the figure. The bubbles occupy a surface layer of thickness d, say, that is usually thin compared with the depth $|Z|$ of the source/receiver. An elementary calculation shows that, if the angle η is substituted for θ, the leading-order error is of of the order of $2(d/|Z|)\cos^2 \eta/\sin \eta$ which is small for small $d/|Z|$ and, actually, exactly zero for $\eta = \pi/2$. Hence, approximately

$$\int_{\mathbf{R}_r}^\mathbf{x} \kappa(\mathbf{y})dl_y = F(0) - \frac{1}{2} F(z). \quad (20)$$

Finally, again due to the smallness of $d/|Z|$, we substitute the distance R of **R** from dS' in place of both denominators in (14) to find the following expression for the incoherent intensity due to the bubbly column of cross-sectional area dS'

$$|p_{\text{inc}}|^2 = \frac{1}{(4\pi)^3 R^4} \int_{-\infty}^{0} S_s\{\exp[-F_I(z)]$$

$$+ \exp[-2F_I(0) + F_I(z)] + 2\, \exp[-F_I(0)]$$

$$\times \cos[\phi + F_R(z) - F_R(0)]\}^2 dz, \tag{21}$$

where we have set

$$F(z) = F_R(z) - iF_I(z), \tag{22}$$

and the integral has been extended to $-\infty$ although, as noted before, the bubble density becomes negligible below a finite depth that is actually small with respect to $|Z|$.

The backscattering strength is defined by (see, e.g., Urick, 1967)

$$\Sigma_B = \frac{R^2 I_s}{I_i \Delta A}, \tag{23}$$

with I_i and I_s the incident and scattered intensities, ΔA the ensonified surface area, and R the distance between the source/receiver and ΔS. From (21) we therefore find

$$\Sigma_B = \frac{1}{4\pi} \int_{-\infty}^{0} S_s\{\exp[-2F_I(z)] + 4\, \exp[-2F_I(0)]$$

$$+ \exp(-2[2F_I(0) - F_I(z)]) + 8\, \exp[-2F_I(0)]$$

$$\times \cos[F_R(0) - F_R(z) - \phi]\cosh[F_I(0) - F_I(z)]$$

$$+ 2\, \exp[-2F_I(0)]\cos\, 2[F_R(0) - F_R(z) - \phi]\}dz. \tag{24}$$

Before proceeding to discuss the results of other researchers mentioned in the Introduction in the light of these expressions, it is useful to note the following approximation to the function F that arises by use of the binomial expansion for the calculation of κ from (2)

$$\kappa \approx k + \frac{1}{2k} \int_{a_{\min}}^{a_{\max}} h(a,\omega;x)N(a,z)da, \tag{25}$$

from which

$$F_R(z) \approx 2k(z-Z) + \frac{1}{\sin\, \eta} \int_{-\infty}^{z} dz \int_{a_{\min}}^{a_{\max}} \left[\left(\frac{\omega_0}{\omega} \right)^2 - 1 \right] \frac{\sigma_s}{ka}$$

$$\times N(a,z)da, \tag{26}$$

$$F_I(z) \approx \frac{1}{\sin\, \eta} \int_{-\infty}^{z} dz \int_{a_{\min}}^{a_{\max}} \sigma_e N(a,z)da, \tag{27}$$

where the scattering cross section of each bubble σ_s is given by (11) and the extinction cross-section σ_e is given by

$$\sigma_e = \frac{\delta}{ka}\, \sigma_s = \frac{4\pi\delta a/k}{[(\omega_0/\omega)^2 - 1]^2 + \delta^2}. \tag{28}$$

We have also extended the range of the integrals to $-\infty$ in view of the fact that N vanishes below the bubbly layer. Note
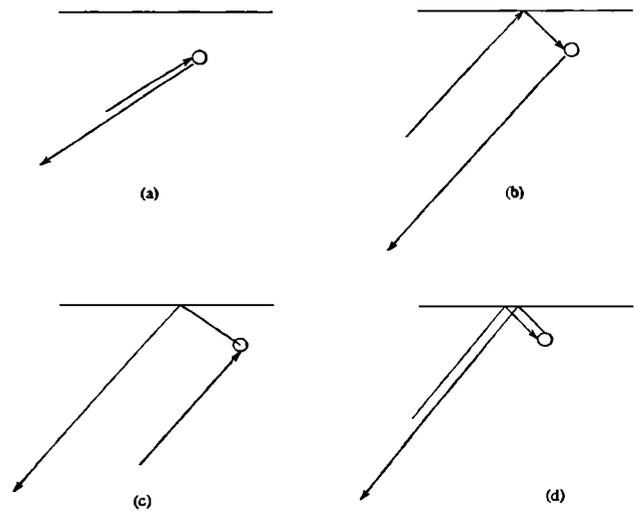
FIG. 3. The four paths by which a bubble can cause backscattering in the ray approximation of Sec. IV.

that, analogously to (10), the extiction cross section per unit volume is

$$S_e = \int_{a_{\min}}^{a_{\max}} \sigma_e N(a,z)da, \tag{29}$$

so that

$$F_I(z) \approx \frac{1}{\sin\, \eta} \int_{-\infty}^{z} S_e(z')dz'. \tag{30}$$

The combination ka in the definition (28) of σ_e is the acoustic radiation damping. In the literature this is sometimes evaluated at resonance and considered constant (McDaniel and Gorman, 1982, 1983; Vagle and Farmer, 1992). The results presented below in Sec. VI indicate that this approximation is likely to be inaccurate.

IV. RAY-ACOUSTIC INTERPRETATION

For a better understanding of the relation of the result (24) to that of others and to gain some insight into the origin of the differences it is useful to interpret it in terms of ray acoustics following the approach of Crowther (1980) and McDaniel (1987).

Consider a single bubble at a position $z < 0$ below the free surface of the ocean. There are four paths, or rays, by which this bubble can contribute to the backscattered intensity, which are shown in Fig. 3 (McDaniel, 1987). The first one, Fig. 3(a), involves the direct scatter of radiation by the bubble. For a source of unit strength, the backscattered pressure amplitude due to this contribution is

$$p_a = \frac{1}{4\pi R^2} \exp\left(-\frac{i}{2} F(z) \right) h\, \exp\left(-\frac{i}{2} F(z) \right). \tag{31}$$

The first exponential is the pressure field exciting the bubble, h is the scattering form factor defined in (3), and the second exponential is the amplitude returning back to the source. The forward part of the path carries the spherical spreading factor $4\pi R$, while the corresponding factor for the backward

part is h/R. The last path, Fig. 3(d), involves two surface reflections and gives the contribution

$$p_d = \frac{1}{4\pi R^2} \exp\left(-\frac{i}{2}F(0)\right)\exp(i\phi)$$

$$\times\exp\left(-\frac{i}{2}[F(0)-F(z)]\right)h\,\exp\left(-\frac{i}{2}[F(0)-F(z)]\right)$$

$$\times\exp(i\phi)\exp\left(-\frac{i}{2}F(0)\right),\qquad(32)$$

where the factors $\exp i\phi$ account for the reflections from the free surface. Here the spherical spreading factor is not exact, but assumes that the depth of the bubble is small compared with its distance from the source.

For the second and third paths, Fig. 3(b) and (c) the sound is scattered by the bubble and undergoes one reflection at the free surface. The contribution of these rays is therefore equal, $p_b = p_c = \sqrt{p_a p_d}$.

The total mean-square pressure field incoherently back-scattered to the source must be calculated by combining the effects of all the bubbles and is therefore proportional to

$$|p_{inc}|^2 = \int_{-\infty}^{0} dz \int_{a_{min}}^{a_{max}} da\ N(a,z)|p_a + p_b + p_c + p_d|^2.\qquad(33)$$

Since, for an isotropic scatterer, $|h|^2 = 4\pi\sigma_s$, it is readily seen that this result is identical to the previously derived one (24). An equivalent form is

$$|p_{inc}|^2 = \int_{-\infty}^{0} dz \int_{a_{min}}^{a_{max}} da\ N(a,z)|\sqrt{p_a} + \sqrt{p_d}|^4$$

$$= \int_{-\infty}^{0} dz \int_{a_{min}}^{a_{max}} da\ N(a,z)|p_a|^2$$

$$\times|1 + \exp i[F(z)-F(0)+\phi]|^4.\qquad(34)$$

It might be noted that, due to the surface wave motion (that they follow to a variable degree depending on their depth), the bubbles' distance from the source changes in time. However, since this motion is effectively "frozen" on the acoustic time scale, its only effect would be to endow each bubble with another phase factor similar to the ϕ introduced earlier. Since the contribution of all four paths is proportional to $|h|^2$, the final result is independent of this phase as found before in the WKB approach.

V. BACKSCATTERING

Crowther (1980), McDaniel and Gorman (1982, 1983), and McDaniel (1987) have calculated the backscattering strength due to a surface bubble layer per unit area of the ocean by the ray-acoustic method outlined in the previous section.

McDaniel and Gorman (1982, 1983) omitted paths c and d and combined a and b incoherently. In a later study, McDaniel (1987) chose to add all the four paths incoherently by calculating, in place of (33),

$$\int_{-\infty}^{0} dz \int_{a_{min}}^{a_{max}} da\ N(a,z)(|p_a|^2 + |p_b|^2 + |p_c|^2 + |p_d|^2).$$

$$(35)$$

In this way she finds the following expression for the back-scattering strength

$$\Sigma_B = \frac{1}{4\pi} \int_{-\infty}^{0} S_s(z)\{\exp[-2g(z)] + 2\exp[-2g(0)]$$

$$+\exp-2[2g(0)-g(z)]\}dz,\qquad(36)$$

where the function g is defined by

$$g(z) = \frac{1}{\sin\eta} \int_{-\infty}^{z} S_e(z')dz'.\qquad(37)$$

This definition is formally the same as the approximation (30) of F_I, but McDaniel and Gorman (1982, 1983) calculate S_e including only the effect of resonant bubbles, as will be described presently, and therefore we prefer to use a different symbol.

With the same treatment of extinction, that replaces F_I by g, Crowther's result [his Eq. (22)] coincides with our Eq. (24) provided one takes $\phi=\pi$ (i.e., a completely flat pressure-release ocean surface), and our $\frac{1}{2}[F_R(z)-F_R(0)]$ is substituted by $kz\sin\eta$. Even assuming $\mathrm{Re}(\kappa)=k$, one would have $\frac{1}{2}[F_R(z)-F_R(0)] \simeq kz/\sin\eta$ rather than $kz\sin\eta$.

One can argue that, for short acoustic wavelengths, the contributions of the paths of Fig. 3(a) and (d) should combine incoherently because one is affected (twice) by the surface, while the other one is unaffected. For a similar reason, the paths of Fig. 3(b) and (c) should combine incoherently with the other two. However, it appears that combining the two paths of Fig. 3(b) and (c) incoherently is incorrect because this is in fact one and the same path, and irrespective of the nature of the surface reflection, it will affect both rays in exactly the same way. If, on the basis of this argument, Σ_B is computed from

$$\int_{-\infty}^{0} dz \int_{a_{min}}^{a_{max}} da\ N(a,z)(|p_a|^2 + |p_b + p_c|^2 + |p_d|^2),\qquad(38)$$

the result is

$$\Sigma_B = \frac{1}{4\pi} \int_{-\infty}^{0} dz\ S_s\{\exp[-2F_I(z)] + \exp(-2[2F_I(0)$$

$$-F_I(z)]) + 4\exp[-2F_I(0)]\}.\qquad(39)$$

The proper way in which (36) and (39) should be compared with our result (24) is after averaging the latter over the phase ϕ. Indeed, if the acoustic wavelength is shorter than the linear dimensions of the insonified surface area, due to the presence of surface waves, the distance of the source from each point on the surface fluctuates about R by an amount that is small compared with R, but not compared with the acoustic wavelength. In this case, different points of the interface would be reached by acoustic wavelets having a randomly distributed phase, and the observed backscattering signal would effectively be the average over these phases. A parallel argument could be developed in a time-averaging
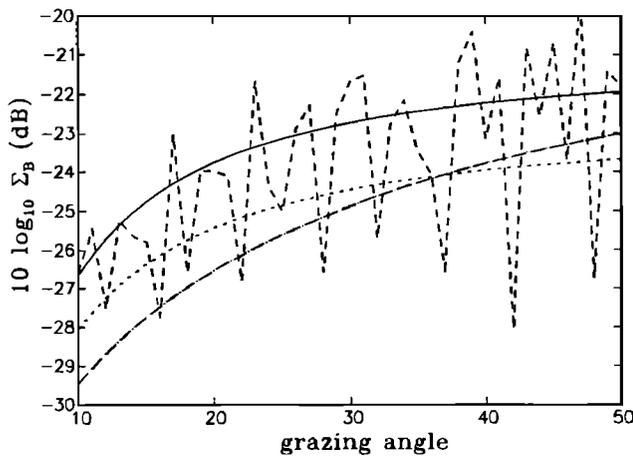
FIG. 4. Comparison of different results for the for the backscattering intensity as functions of the grazing angle in degrees at 20 kHz. The solid line is the present expression (39). The short-dash line is (35) (McDaniel, 1987). The oscillating dashed line is (24) with $\phi=\pi$ (Crowther, 1980). The bubble distribution used here is that of McDaniel (1987), $N(a,z)$ $=(n_0/a^{4.3})\exp(z/L)$, with $L=1$ m (appropriate for a wind speed of 30 knots), $n_0=3.27\times10^{-9}$, with the radius integration effected over 50 $\mu m \leqslant a \leqslant 500$ μm. For a value of n_0 100 times as large, $n_0=3.27\times10^{-7}$, the three results coincide (dash-and-dot line) due to the saturation effect described in the Appendix.

FIG. 5. Logarithmic decrement δ as a function of the ratio of the sound frequency to the bubble resonance frequency ω_0 for four different bubble radii.

sense. Our result (24) is readily averaged over ϕ and the result is then identical to (39).

The two different derivations that we have provided for the result (39)—one from Foldy's theory, the other by a direct application of ray acoustics—lend support to its validity as opposed to that of (35) or (36). While the difference between the two expressions has some conceptual significance, quantitatively the effect is not large once the result is expressed in dB. We show in Fig. 4 a comparison of (24) with $\phi=\pi$ and (35) with (38) or (39) as a function of the grazing angle η at 20 kHz. The bubble distribution used here is that of McDaniel (1987), $N(a,z)=(n_0/a^{4.3})\exp(z/L)$, with $L=1$ m (appropriate for a wind speed of 30 knots), $n_0=3.27\times10^{-9}$ cm$^{-8.3}$ (a in cm), with the radius integration effected over 50 $\mu m \leqslant a \leqslant 500$ μm. The corresponding volume fraction is given by $\beta=34.14$ $n_0 \exp(z/L)$. The solid line shows (39), the dashed line (35), and the highly oscillating dashed line (24) with $\phi=\pi$. For a value of n_0 100 times as large, $n_0=3.27\times10^{-7}$, all three results coincide (dash-and-dot line) due to the saturation effect described in the Appendix.

VI. EFFECT OF THE BUBBLE SPECTRUM

The second point that we wish to address is the manner in which the contribution of the extinction and scattering cross sections to the various integrals over the bubble radius distribution arising in the theory is usually evaluated. The basic approximation (Wildt, 1946; see also Medwin, 1970, 1977a,b,c; Clay and Medwin, 1991) gives

$$S_s \simeq (\pi/2)\delta_R a_R N(a_R,z)\sigma_{sR},\tag{40}$$

$$S_e \simeq (\pi/2)\delta_R a_R N(a_R,z)\sigma_{eR},\tag{41}$$

where the subscript R indicates resonance values, i.e., values corresponding to the insonifying frequency ω. In particular, $a_R(\omega)$ is such that ω_0 given by (4) equals ω. A derivation of these results is given in the Appendix, which also contains more accurate estimates for a power-law bubble spectrum of the form

$$N(a,z)=N_0(z)a^{-n}.\tag{42}$$

A relation of this type has been proposed by several researchers who suggest values for n between 2.6 (Medwin and Breitz, 1989) and 6 (Su *et al.*, 1988; Farmer and Vagle, 1989), with most results in the range 3 to 5 (Blanchard and Woodcock, 1957; Farmer and Lemon, 1984; Johnson and Cooke, 1979; Kolovayev, 1976; Walsh and Mulhearn, 1987). The results (40) and (41) are obtained on the assumption that σ_s is strongly peaked around $\omega=\omega_0$, a region where the logarithmic decrement δ is also small (see Fig. 5). Although the same method is used to obtain (41), it should be noted that, in view of the relation (28) between σ_s and σ_e, the latter quantity is less peaked than σ_s and is, actually, relatively large below resonance. Thus one expects that the error in-
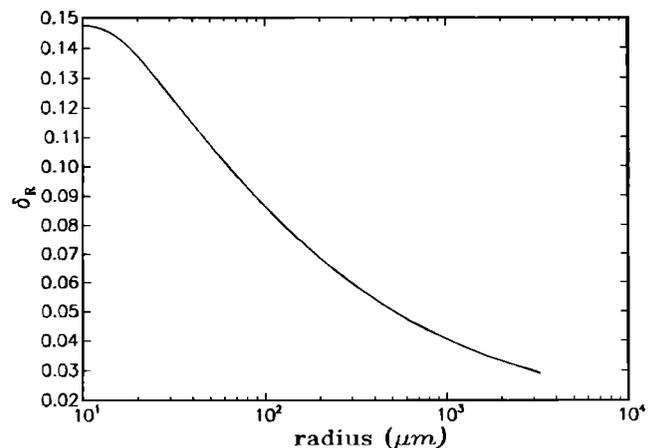
FIG. 6. Resonance value δ_R of the logarithmic decrement δ as a function of the bubble equilibrium radius a.

K. Sarkar and A. Prosperetti: Coherent and incoherent scattering
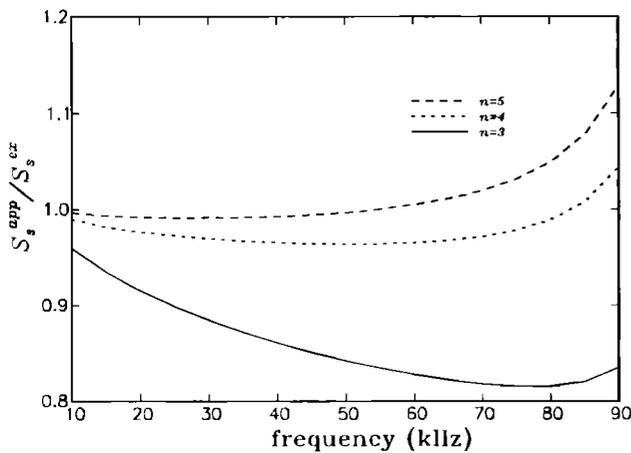
FIG. 7. Ratio of the approximation (40) for the scattering cross section to the exact result obtained by numerical evaluation of the integral (10) as a function of the sound frequency. The bubble spectrum is the power law (42) and the integration over the bubble radii has been carried out from 30 μm to 1 mm.

curred in keeping δ constant in this region (Fig. 6) will adversely affect the accuracy of (41).

We now compare these approximations with the result of a numerical evaluation of the integrals in (10) and (29) with the correct expressions for ω_0 and all the other quantities appearing in the formulae. Figure 7 shows the ratio between the approximation (40) and the exact numerical result for a power law of the form (42) with $n = 3$, 4, and 5. Figure 8 is the analogous result for the extinction cross section. In both cases the radius integration has been carried out over the range 30 μm$\leq a \leq 1$ mm. For the three values of n one has $\beta = 0.4063$ $N_0(z)$, 14.69 $N_0(z)$, and 1354 $N_0(z)$. It is seen here that the approximation (40) may not be very good at the higher frequencies if n is small. The reason for this behavior is given in the Appendix. As anticipated, the approximation (41) is poorer for S_e (note the different scale in the figures). The error at the lower frequencies is of particular concern since S_e appears as argument of an exponential in (37).
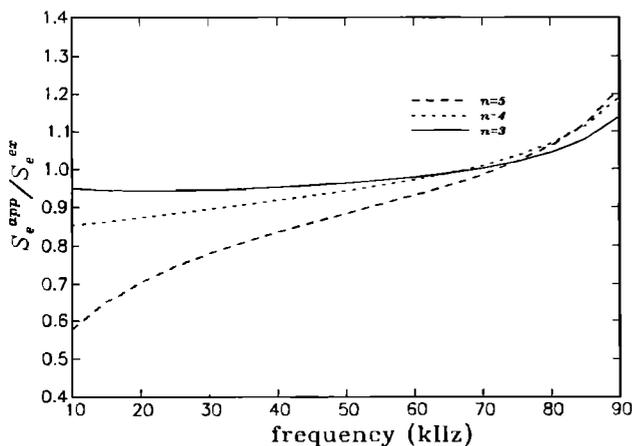
FIG. 8. Ratio of the approximation (41) for the extinction cross section to the exact result obtained by numerical evaluation of the integral (29) as a function of the sound frequency. The bubble spectrum is the power law (42) and the integration over the bubble radii has been carried out from 30 μm to 1 mm.
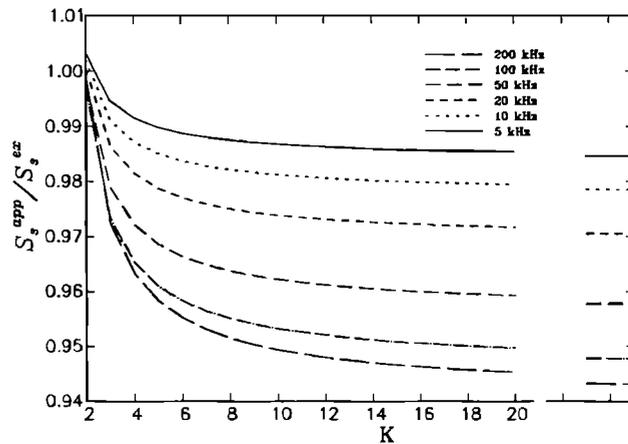
FIG. 9. Saturation effect of the ratio between the approximate and exact scattering cross sections as a function of the width of the radial integration. The parameter K is defined in Eq. (43).

The previous results depend on the range of the integration over radii. Figures 9 and 10 illustrate this effect for several frequencies for a power spectrum of the form (42) with $n = 4$. Here, for each frequency, the integration is carried out for

$$(1/K)a_R \leq a \leq K a_R, \tag{43}$$

and the results are plotted as a function of K. The resonant radii at the frequencies 5, 10, 20, 50, 100, 200 kHz are 645, 321, 159, 62.5, 30.8, 15.2 μm, respectively. While a saturation effect is clear as the integration range increases, there is a rather steep dependence over smaller ranges. Because of this range dependence, the correspondence between these results and and those of Figs. 7 and 8 is not exact at all frequencies.

Another point worth noting is the strong error that is encountered for frequencies near the resonant frequency of the smallest and largest bubbles in the distribution. This is illustrated in Fig. 11 for the two ranges 20 μm$\leq a \leq 1.2$ mm, and 30 μm$\leq a \leq 200$ μm. For the wider range the natural frequencies corresponding to the endpoints are 152.5 and
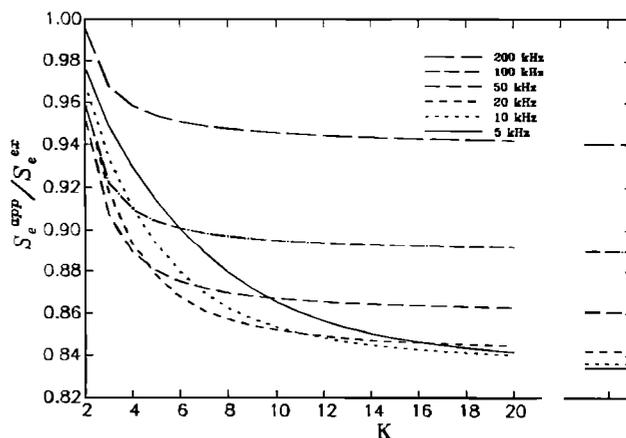
FIG. 10. Saturation effect of the ratio between the approximate and exact extinction cross sections as a function of the width of the radial integration. The parameter K is defined in Eq. (43).
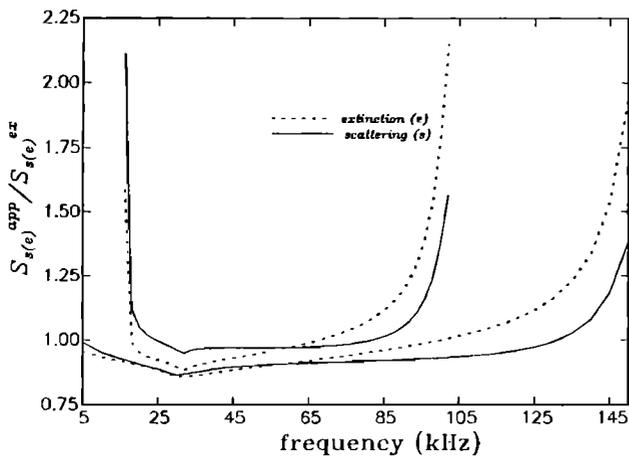
FIG. 11. Ratio of the approximations (40) and (41) to the exact results as a function of the sound frequency for two different ranges of radial integration, $20 \ \mu\text{m} \leqslant a \leqslant 1.2$ mm, and $30 \ \mu\text{m} \leqslant a \leqslant 200 \ \mu\text{m}$. The bubble spectrum is the power law (42) with $n=4$ up to $a=100 \ \mu\text{m}$, and $n=3$ above.

2.701 kHz, respectively, for the shorter one 102.6 and 15.9 kHz. For this example we have used the power-law (42) with $n=4$ up to $a=100 \ \mu\text{m}$ and $n=3$ above. The slight slope discontinuities in the curves arise from the switching between these two expressions. The volume fraction corresponding to the wider range is given by $\beta=52.82N_0(z)$.

The suggestion has been made (e.g., McDaniel, 1987) that the approximation implicit in (40), (41) can be corrected by the use of a constant multiplicative factor. The previous results illustrate the possible shortcomings of this approach.

Finally, we consider the effect of the use of the binomial expansion (25) to derive the backscattering formula. We examine the accuracy of this approximation in Fig. 12 which shows the ratio of the imaginary part of κ according to (25) to the exact numerical value as a function of N_0 defined in Eq. (42) as a parameter. These calculations have been carried out for the broader one of the two spectra used for Fig. 11. The three lines are for $\omega/2\pi=10$, 50, and 100 kHz in descending order. The gas volume fraction is approximately
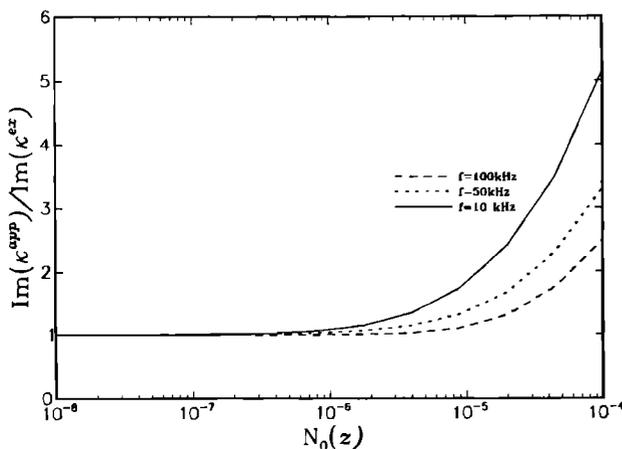
FIG. 12. Ratio of the imaginary part of the mixture wave number according to the binomial expansion (25) to the exact value given by (2) as a function of the parameter N_0 appearing in Eq. (42). These results are for the same bubble spectrum used in the previous figure. The corresponding volume fraction is given by $52.8 \ N_0$, approximately.

equal to $52.82N_0$, so that the right boundary of the figure corresponds to a total gas content of about 0.5%. It is seen that, even for such a relatively small concentration, the error is a factor of 5. It is clear that only extremely small gas concentrations can be treated with this approximation.

VII. BUBBLE COUNTING BY ACOUSTIC SCATTERING

One of the techniques developed for the in situ acoustic measurement of bubble density and size distribution uses incoherent scattering and can be analyzed with the previous ideas. The method is essentially the following (see Medwin, 1970, 1977a,b; Thorpe, 1982; Vagle and Farmer, 1992). If an upward-pointing sonar sends a short high-frequency pulse toward the ocean surface, it is found that the reflection of the main pulse by the surface (or by the dense bubble layer in its immediate neighborhood) is preceded by a nearly continuous, much weaker signal that is interpreted as the incoherent backscattering due to the bubbles that the pulse encounters on its way to the surface. Assuming that the sound speed is not significantly affected by the presence of these bubbles, the part of the signal received between t and $t+\Delta t$ is attributed to the bubbles at a distance from the transducer given by the travel time of the pulse. From the amplitude of this part of the signal one can infer the bubble number at that location.

The application of the preceding method to the analysis of this case is simpler than before, as the presence of the free surface is inessential here due to the time "gating" so that Eqs. (14) and (15) can be used without the second term and Eq. (13) gives, with the same approximations as in Sec. III,

$$|p_{\text{inc}}|^2 = \frac{1}{(4\pi)^3 R^4} S_s \exp[-2F_I(z)].$$ (44)

For a sufficiently small bubble concentration $F_I \approx 0$ and it is seen from this relation that the reduction of the backscattered data by the technique mentioned before amounts essentially to a measurement of S_s at different positions in space and different frequencies. From this information the bubble size spectrum can be determined. The neglect of the exponential attenuation can be avoided (Vagle and Farmer, 1992) by noting that, after the bubble distribution and density at the closest z has been obtained, the attenuation of the beam reaching the next level can be estimated and so on.

The recovery of the bubble size distribution from these data requires the solution of Eq. (10) considered as a Fredholm integral equation of the first kind in $N(a,x)$. The method traditionally used for this purpose has been the resonant bubble approximation of the Appendix and Sec. VI (Medwin, 1970, 1977a,b). Commander and Moritz (1989) have studied the accuracy of this approach and found appreciable discrepancies in some cases, particularly for the smaller bubbles of the population. Commander and Mc-Donald (1991) and, more recently, Duraiswami (1993), described a more precise numerical method that deals effectively with the ill-posed nature of the problem. Vagle and Farmer (1992) use six frequencies and the resonant approxi-

mation would be too crude in this case. They describe several inversion methods suitable for this relatively small number of frequencies.

Without entering into the issue of the solution of the integral equation, which has been dealt with sufficiently in the literature, we simply point out that the bubble-counting procedure just described relies on the assumption that the coherent field is not reflected before it reaches the surface and all of the measured backscattered signal is incoherent. This is of course implicit in the use of the lowest-order WKB approximation. We have tested this assumption by solving numerically Eq. (1) for several bubble number distribution functions $N(a,z)$. In all cases we have set $N(a,z)=N_1(a)f(z)$. For the a dependence, we have used the distribution of Figs. 11 and 12 normalized so as to give several values of the total volume fraction β. For the z dependence we have tested several forms of which the following ones are typical:

$$f(z)=1/2[1+\tanh(z/l)][1+\epsilon \sin (2\pi z/l_1)], \quad (i)$$

$$f(z)=\exp(-z^2/l_2^2). \quad (ii)$$

The length l was varied between 0.05 and 0.5 m, the length l_1 between 0.05 and 0.1 m, the length l_2 between 0.1 and 1 m, and ϵ between 0 and 0.5, with gas volume fractions up to 0.1%. In all cases we found that the reflection of the coherent signal was quite negligible thus substantiating the assumption implicit in the previous procedure.

VIII. SUMMARY AND CONCLUSIONS

The point of departure of this study has been to show that a WKB approximation applied to the effective-medium description of sound propagation in bubbly liquids gives results completely equivalent to those of a description in terms of incoherent scattering. This idea is then applied to two problems, surface backscattering and acoustical bubble counting.

It has been shown that earlier theories of backscattering by superficial bubble distributions are contained in the formulation of this paper as approximations or special cases. A numerical illustration of the differences among these results has been given. Essentially, they all agree within a few dB. Earlier theories also used other approximations in the calculation of the bubble contribution, and notably the idea that only resonant bubbles are significant. Our analysis of this approximation indicates that it should be used with great care as large errors may be incurred. The behavior of the error is also strongly dependent on the bubble size spectrum so that general conclusions cannot be derived.

For the acoustical bubble counting problem, we have shown that the current practice, which is based on the neglect of the coherently reflected field, is likely to be accurate.

ACKNOWLEDGMENTS

APPENDIX

For any given angular frequency ω, from Eq. (4) one can define a resonant radius $a_R(\omega)$ and logarithmic decrement $\delta_R(\omega)$. If the function Ψ appearing in the expressions (4), (5) of the resonance frequency and damping were independent of a and ω and surface tension effects were negligible then, from (4), one would have $\omega_0/\omega=a_R/a$ so that the scattering cross section per unit volume (10) would be given by

$$S_s \approx 4 \pi a_R^4 \int_{a_R/a_{max}}^{a_R/a_{min}} \frac{x^{-4}N(a_R/x)}{(x^2-1)^2+\delta^2} \, dx, \quad (A1)$$

where $x=a_R/a$. Although, as shown in Fig. 6, δ is far from constant, for smooth N the greatest contribution to the integral arises from a region of order of magnitude δ around $x=1$. Since, as shown in Fig. 5, δ is small near resonance, this region is narrow and it is therefore reasonable to keep δ constant and equal to its resonance value δ_R in the evaluation of the integral. This remark motivates the further change of variable $y=(x^2-1)/\delta_R$, where again $\delta_R=\delta(\omega)$, to find

$$S_s \approx 2 \pi \frac{a_R^3}{\delta_R} \int_{y_m}^{y_M} \frac{(1+\delta_R y)^{-5/2}}{y^2+1} N(a_R/\sqrt{1+\delta_R y}) \, dy, \quad (A2)$$

where $y_m=[(a_R/a_{max})^2-1]/\delta_R$, $y_M=[(a_R/a_{min})^2-1]/\delta_R$. For $\delta_R \to 0$ $y_m \to -\infty$, $y_M \to \infty$, so that

$$S_s \approx 2 \pi^2 N(a_R,z)(a_R^3/\delta_R), \quad (A3)$$

from which, with $\sigma_{sR}=4\pi(a_R/\delta_R)^2$, the result (40) is obtained. A similar procedure leads to (41).

A consideration of the form (A1) of the integral gives an explanation of the fact, noted in Sec. VI, that the approximation (40) fails at high frequency for small n. Indeed, at high frequency, a_R is small and the range of integration restricted therefore to a small interval near $x=0$. If n is small, the decline of N as $x \to 0$ is not sufficient to balance the factor x^{-4} and the integral becomes large, while the approximate result is little affected. The ratio of the two quantities therefore becomes small as seen in Fig. 7.

It may be of some interest to note that the integration in (A1) and the analogous one for the extinction cross section can be carried out in closed form for a power-law bubble spectrum provided $a_{min}=0$, $a_{max}=\infty$ and δ is kept constant. Standard contour integration (see, e.g., Whittaker and Watson, 1927) gives

$$\int_0^\infty \frac{x^{n-4} \, dx}{(x^2-1)^2+\delta^2}$$

$$=\frac{\pi}{2\delta} (1+\delta^2)^{(n-5)/4} \frac{\sin \frac{1}{4}[(n-3)\pi-(n-5)\alpha]}{\sin \frac{1}{2}(n-3)\pi}, \quad (A4)$$

where $\sin \alpha = \delta/\sqrt{1+\delta^2}$. The integral exists for $3<n<7$. The similar integral involved in the calculation of S_e converges for $2<n<6$ and therefore $3<n<6$ for both integrals to converge. It is readily seen that, for small δ, the leading order contribution is $(\pi/2)\delta$, which leads to the approximations (40) and (41).

While not always accurate, the binomial expansion (25) for the calculation of the effective wave number allows one to quickly obtain some insight into the basic trends of the results of the more complex precise formulae. For this reason it is of some interest to apply it to the backscattering strength (39) with the additional assumption that the bubble distribution $N(a,z)$ factors into a product, $N(a,z) = N_1(a)f(z)$. Following the development given by McDaniel and Gorman (1982) we find

$$\Sigma_B \simeq \frac{\hat{S}_s}{4\pi} \left\{ 4\psi \exp\left(-\frac{2}{\sin \eta} \hat{S}_e \psi \right) \right.$$

$$\left. + \frac{\sin \eta}{2\hat{S}_e} \left[1 - \exp\left(-\frac{4}{\sin \eta} \hat{S}_e \psi \right) \right] \right\}, \qquad (A5)$$

where we have set $\psi = \int_{-\infty}^{0} f \, dz$ and $\hat{S}_{s,e} = S_{s,e}(\omega, z=0)/f(z=0)$. If the attenuation is large this expression reduces to the saturation limit

$$\Sigma_B \simeq (\hat{S}_s/8\pi\hat{S}_e)\sin \eta, \qquad (A6)$$

or, with the resonant radius approximation,

$$\Sigma_B \simeq (ka_R/8\pi\delta_R)\sin \eta. \qquad (A7)$$

This expression coincides with that of McDaniel and Gorman (1982) except for their correction factor 1.7. In the opposite limit of small attenuation the result is

$$\Sigma_B \simeq 3(\hat{S}_s/2\pi)\psi \simeq 3\pi(a_R^3/\delta_R)\psi, \qquad (A8)$$

which is three times the result of McDaniel and Gorman (1982), again except for their correction factor 1.7. These considerations show that the difference between (39) and (35) vanish as the attenuation caused by bubbles increases.

Blanchard, D. C., and Woodcock, A. H. (1957). "Bubble formation and modification in the sea and its meteorological significance," Tellus 9, 145–158.

Carey, W. M., and Bradley, M. P. (1985). "Low-frequency ocean surface noise sources," J. Acoust. Soc. Am. Suppl. 1 78, S1–S2.

Carey, W. M., and Browning, D. (1988). "Low-frequency ocean ambient noise: Measurement and theory," in Sea Surface Sound, edited by B. R. Kerman (Kluwer, Dordrecht), pp. 361–376.

Carey, W. M., and Roy, R. A. (1993). "Sound scattering from microbubble distributions near the sea surface," in Proceedings of the SACLANT Symposium on Ocean Reverberation (Kluwer, Dordrecht, in press).

Clay, C. S., and Medwin, H. (1964). "High-frequency acoustical reverberation from a rough-sea surface," J. Acoust. Soc. Am. 36, 2131–2134.

Clay, C. S., and Medwin, H. (1991). Acoustical Oceanography (Wiley, New York), 2nd ed.

Commander, K. W., and Moritz, E. (1989). "Off-resonance contributions to acoustical bubble spectra," J. Acoust. Soc. Am. 85, 2665–2669.

Commander, K. W., and McDonald, R. J. (1991). "Finite-element solution of the inverse problem in bubble swarm acoustics," J. Acoust. Soc. Am. 89, 592–597.

Commander, K. W., and Prosperetti, A. (1989). "Linear pressure waves in bubbly liquids: Comparison between theory and experiment," J. Acoust. Soc. Am. 85, 732–746.

Crowther, P. A. (1980). "Acoustical scattering from near-surface bubble layers" in Cavitation and Inhomogeneities in Underwater Acoustics, edited by W. Lauterborn (Springer, Berlin), pp. 194–204.

Duraiswami, R. (1993). "Bubble density measurement using an inverse acoustic scattering technique," in Cavitation and Multiphase Flow Forum 1993, edited by O. Furuya (American Society of Mechanical Engineers, New York), pp. 67–73.

Farmer, D. M., and Lemon, D. D. (1984). "The influence of bubbles on ambient noise in the ocean at high wind speeds," J. Phys. Ocean. 14, 1762–1778.

Farmer, D. M., and Vagle, S. (1989). "Waveguide propagation of ambient sound in the ocean surface bubble layer," J. Acoust. Soc. Am. 86, 1897–1908.

Foldy, L. L. (1945). "The multiple scattering of waves, I. General theory of isotropic scattering by randomly distributed scatterers," Phys. Rev. 67, 107–119.

Johnson, B. D., and Cooke, R. C. (1979). "Bubble populations and spectra in coastal water: a photographic approach," J. Geophys. Res. 84, 3761–3766.

Kolovayev, P. A. (1976). "Investigation of the concentration and size distribution of wind-produced bubbles in the near-surface ocean layer," Oceanology 15, 659–661.

McDaniel, S. T., and Gorman, A. D. (1982). "Acoustic and radar sea surface back scatter," J. Geophys. Res. 87, 4127–4136.

McDaniel, S. T., and Gorman, A. D. (1983). "Spectral spread of sea-surface reverberation," J. Acoust. Soc. Am. 74, 241–248.

McDaniel, S. T. (1987). "Vertical spatial coherence of backscatter from bubbles," IEEE J. Oceanic Eng. 12, 349–356.

Medwin, H. (1970). "In situ acoustic measurements of bubble populations in coastal ocean waters" J. Geophys. Res. 75, 599–611.

Medwin, H. (1977a). "Acoustical determinations of bubble-size spectra," J. Acoust. Soc. Am. 62, 1041–1044.

Medwin, H. (1977b). "Counting bubbles acoustically: a review." Ultrasonics 15, 7–13.

Medwin, H. (1977c). "In situ acoustic measurements of microbubbles at sea," J. Geophys. Res. 82, 971–976.

Medwin, H., and Breitz, N. D. (1989). "Ambient and transient bubbles spectra densities in quiescent seas and under spilling breakers," J. Geophys. Res. 94, 12,751–12,759.

Morse, P. M., and Feshbach, H. (1953). Methods of Theoretical Physics (McGraw, New York), Vol. II.

Nicholas, M., Roy, R. A., Crum, L. A., Oğuz, H. N., and Prosperetti, A. (1994). "Sound emission by a laboratory bubble cloud," J. Acoust. Soc. Am. (in press).

Prosperetti, A., Crum, L. A., and Commander, K. W. (1988). "Nonlinear bubble dynamics," J. Acoust. Soc. Am. 83, 502–514.

Prosperetti, A. (1991). "The thermal behaviour of oscillating gas bubbles," J. Fluid Mech. 222, 587–616.

Prosperetti, A., Lu, N. Q., and Kim, H. S. (1993). "Active and passive acoustic behavior of bubble clouds at the ocean's surface," J. Acoust. Soc. Am. 93, 3117–3127.

Sarkar, K., and Prosperetti, A. (1993). "Backscattering of underwater noise by bubble clouds," J. Acoust. Soc. Am. 93, 3128–3138.

Su, M.-Y., Ling, S. C., and Cartmill, J. (1988). "Optical microbubble measurements in the North Sea," in Sea Surface Sound, edited by Kerman, B R. (Kluwer, Dordrecht), pp. 211–224.

Thorpe, S. (1982). "On the clouds of bubbles formed by breaking waves in deep waters in deep water and their role in air–sea gas transfer," Philos. Trans. R. Soc. London Ser. A 304, 155–210.

Twersky, V. (1964). "On propagation in random media of discrete scatterers," in Stochastic Processes in Mathematical Physics and Engineering, edited by R. Bellman (American Mathematical Society, Providence), pp. 84–116.

Urick, R. J. (1967). Principles of Underwater Sound for Engineers (McGraw, New York), Chap. 8.

Vagle, S., and Farmer, D. M. (1992). "The measurement of bubble-size distributions by acoustical backscatter," J. Atmos. Ocean. Tech. 9, 630–644.

Walsh, A. L., and Mulhearn, P. J. (1987). "Photographic measurements of bubble populations form breaking wind waves at sea," J. Geophys. Res. 92C, 14,553–14,565.

Wildt, R. (1946). Ed., Physics of Sound in the Sea, Chap. 28 "Acoustic theory of bubbles," N.D.R.C., Summary Tech. Rep., Div. 6, Vol. 8, Department of Defense, Washington DC.

Whittaker, E. T., and Watson G. N. (1927). A Course of Modern Analysis (Cambridge U.P., Cambridge).

Yoon, S. W., Crum, L. A., Prosperetti, A., and Lu, N. Q. (1991). "An investigation of the collective oscillations of a bubble cloud," J. Acoust. Soc. Am. 89, 700–706.